Supplementary Information for Large-scale features and evaluation of the PMIP4-CMIP6 *midHolocene* simulations

Chris M. Brierley[1], Anni Zhao[1], Sandy P. Harrison[2], Pascale Braconnot[3], Charles J. R. Williams[4,5], David J. R. Thornalley[1], Xiaoxu Shi[6], Jean-Yves Peterschmitt[3], Rumi Ohgaito[7], Darrell S. Kaufman[8], Masa Kageyama[3], Julia C. Hargreaves[9], Michael P. Erb[8], Julien Emile-Geay[10], Roberta D'Agostino[11], Deepak Chandan[12], Matthieu Carré[13,14], Partrick Bartlein[15], Weipeng Zheng[16], Zhongshi Zhang[17], Qiong Zhang[18], Hu Yang[6], Evgeny M. Volodin[19], Robert A. Tomas[20], Cody Routson[8], W. Richard Peltier[12], Bette Otto-Bliesner[20], Polina A. Morozova[21], Nicholas P. McKay[8], Gerrit Lohmann[6], Allegra N. Legrande[22], Chuncheng Guo[17], Jian Cao[23], Esther Brady[20], James D. Annan[9], and Ayako Abe-Ouchi[7,24]

[1]Department of Geography, University College London, London, WC1E 6BT, UK
[2]Department of Geography and Environmental Science, University of Reading, Reading, RG6 6AB, UK
[3]Laboratoire des Sciences du Climat et de l'Environnement-IPSL, Unité Mixte CEA-CNRS-UVSQ, Université Paris-Saclay, Orme des Merisiers, Gif-sur-Yvette, France
[4]Department of Meteorology, University of Reading, Reading, RG6 6BB, UK
[5]School of Geographical Sciences, University of Bristol, University Road, Bristol, BS8 1SS, UK
[6]Alfred-Wegener-Institut Helmholtz-Zentrum f ur Polar- und Meeresforschung, Bremerhaven, Germany
[7]Japan Agency for Marine-Earth Science and Technology, Yokohama, Japan
[8]School of Earth and Sustainability, Northern Arizona University, Flagstaff, AZ 86011, USA.
[9]Blue Skies Research Ltd, The Old Chapel, Albert Hill, Settle, BD24 9HE, UK
[10]Department of Earth Sciences, University of Southern California, Los Angeles, California, USA
[11]Max Planck Institute for Meteorology, Hamburg, Germany
[12]Department of Physics, University of Toronto, 60 St George Street, Toronto, Ontario, M5S1A7, Canada
[13]LOCEAN Laboratory, Sorbonne Universités (UPMC, Univ Paris 06)-CNRS-IRD-MNHN, Paris, France
[14]CIDIS-LID-Facultad de Ciencias y Filosofía-Universidad Peruana Cayetano Heredia, Lima, Peru
[15]Department of Geography, University of Oregon, Eugene, OR 97403, USA
[16]LASG, Institute of Atmospheric Physics, Chinese Academy of Sciences, Beijing 100029, China
[17]NORCE Norwegian Research Centre, Bjerknes Center for Climate Research, Bergen, Norway
[18]Department of Physical Geography and Bolin Centre for Climate Research, Stockholm University, 10691, Stockholm, Sweden
[19]Marchuk Institute of Numerical Mathematics, Russian Academy of Sciences, ul. Gubkina 8, Moscow, 119333, Russia
[20]Climate and Global Dynamics Laboratory, National Center for Atmospheric Research (NCAR), Boulder, CO 80305, USA
[21]Institute of Geography, Russian Academy of Sciences, Staromonetny L. 29, Moscow, 110917, Russia
[22]NASA Goddard Institute for Space Studies, 2880 Broadway, New York, NY 10025, USA
[23]School of Atmospheric Sciences, Nanjing University of Information Science & Technology Nanjing, 210044, China
[24]Atmospheric and Ocean Research Institute, The University of Tokyo, Kashiwa, Japan

Correspondence: c.brierley@ucl.ac.uk

Abstract. The mid-Holocene (6,000 years ago) is a standard experiment for the evaluation of the simulated response of global climate models using paleoclimate reconstructions. The latest mid-Holocene simulations are a contribution by the Palaeoclimate Model Intercomparison Project (PMIP4) to the current phase of the Coupled Model Intercomparison Project (CMIP6).

Here we provide an initial analysis and evaluation of the results of the experiment for the mid-Holocene. We show that state-of-the-art models produce climate changes that are broadly consistent with theory and observations, including increased summer warming of the northern hemisphere and associated shifts in tropical rainfall. Many features of the PMIP4-CMIP6 simulations were present in the previous generation (PMIP3-CMIP5) of simulations. The PMIP4-CMIP6 ensemble for the mid-Holocene has a global mean temperature change of -0.3 K, which is -0.2 K cooler that the PMIP3-CMIP5 simulations predominantly as a result of the prescription of realistic greenhouse gas concentrations in PMIP4-CMIP6. Neither this difference nor the improvement in model complexity and resolution seems to improve the realism of the simulations. Biases in the magnitude and the sign of regional responses identified in PMIP3-CMIP5, such as the amplification of the northern African monsoon, precipitation changes over Europe and simulated aridity in mid-Eurasia, are still present in the PMIP4-CMIP6 simulations. Despite these issues, PMIP4-CMIP6 and the mid-Holocene provide an opportunity both for quantitative evaluation and derivation of emergent constraints on climate sensitivity and feedback strength.

Table S1

Key metrics of change in the PMIP4-CMIP6 *midHolocene* simulations, in either absolute terms or as a percentage of the *piControl* simulations. For comparison with the reconstructions when available, the quoted values are the average simulated at site locations only, otherwise they are area-averages. Northern high-latitude land is defined as any land between 50–80°N. Midcontinental Eurasia is defined as 40–60°N, 30–120°E by Bartlein et al. (2017). Central Asia is defined as 30–50°N, 60–75°E (Christensen et al., 2013) and these values appear in Fig. 11. The northward monsoon expansion is calculated by determining the change in latitude where the zonal mean summer (MJJAS) rain rate (Fig. S1) equals 2 mm/day over the North Africa (15°W–30°E). The area-averaged mean annual rainfall changes are computed over 20°S –0°N, 65–45°W for South America, and 25–30°N, 70–85°E for the Indo-Gangetic Plain. ENSO activity is measured by the change in variance of monthly sea surface temperature anomalies in the Niño3.4 region (5°S–5°N, 170–120°W; Brown et al., submitted). The probability of a 50-year record in which pseudocoral ENSO activity is weak as in reconstructions for 3-5ka BP is shown separately for both the *midHolocene* and *piControl* simulations (Emile-Geay et al., 2016). The zonal sea surface temperature (SST) gradient along the Equatorial Pacific is calculated as difference between the annual mean area average over 5°S–5°N,150–190°E and the annual mean area average over 5°S–5°N,240–270°E after Brown et al. (submitted).

References

Adler, R. F., Huffman, G. J., Chang, A., Ferraro, R., Xie, P.-P., Janowiak, J., Rudolf, B., Schneider, U., Curtis, S., Bolvin, D., et al.: The version-2 global precipitation climatology project (GPCP) monthly precipitation analysis (1979–present), Journal of hydrometeorology, 4, 1147–1167, https://doi.org/10.1175/1525-7541(2003)004<1147:TVGPCP>2.0.CO;2, 2003.

Bartlein, P. J., Harrison, S., Brewer, S., Connor, S., Davis, B., Gajewski, K., Guiot, J., Harrison-Prentice, T., Henderson, A., Peyron, O., et al.: Pollen-based continental climate reconstructions at 6 and 21 ka: a global synthesis, Climate Dynamics, 37, 775–802, https://doi.org/10.1007/s00382-010-0904-1, 2011.

Bartlein, P. J., Harrison, S. P., and Izumi, K.: Underlying causes of Eurasian midcontinental aridity in simulations of mid-Holocene climate, Geophysical research letters, 44, 9020–9028, https://doi.org/10.1002/2017GL074476, 2017.

Braconnot, P., Otto-Bliesner, B., Harrison, S., Joussaume, S., Peterchmitt, J.-Y., Abe-Ouchi, A., Crucifix, M., Driesschaert, E., Fichefet, T., Hewitt, C., et al.: Results of PMIP2 coupled simulations of the Mid-Holocene and Last Glacial Maximum–Part 1: experiments and large-scale features, Climate of the Past, 3, 261–277, https://doi.org/10.5194/cp-3-261-2007, 2007.

Braconnot, P., Harrison, S. P., Kageyama, M., Bartlein, P. J., Masson-Delmotte, V., Abe-Ouchi, A., Otto-Bliesner, B., and Zhao, Y.: Evaluation of climate models using palaeoclimatic data, Nature Climate Change, 2, 417, https://doi.org/10.1038/nclimate1456, 2012.

Brown, J., Brierley, C. M., An, S.-I., Guarino, M.-V., Stevenson, S., Williams, C. J. R., et al.: Comparison of past and future simulations of ENSO in CMIP5/PMIP3 and CMIP6/PMIP4 models, Climate of the Past, ?, ???–???, submitted.

Christensen et al.: Climate phenomena and their relevance for future regional climate change [IPCC WG1 AR5 Chap14], 2013.

Emile-Geay, J., Cobb, K. M., Carre, M., Braconnot, P., Leloup, J., Zhou, Y., Harrison, S. P., Correge, T., McGregor, H. V., Collins, M., Driscoll, R., Elliot, M., Schneider, B., and Tudhope, A.: Links between tropical Pacific seasonal, interannual and orbital variability during the Holocene, Nature Geosci, 9, 168–173, https://doi.org/10.1038/ngeo2608, 2016.

Hargreaves, J. C., Annan, J. D., Ohgaito, R., Paul, A., and Abe-Ouchi, A.: Skill and reliability of climate model ensembles at the Last Glacial Maximum and mid-Holocene, Climate of the Past, 9, 811–823, https://doi.org/10.5194/cp-9-811-2013, 2013.

Joussaume, S., Taylor, K., Braconnot, P., Mitchell, J., Kutzbach, J., Harrison, S., Prentice, I., Broccoli, A., Abe-Ouchi, A., Bartlein, P., et al.: Monsoon changes for 6000 years ago: results of 18 simulations from the Paleoclimate Modeling Intercomparison Project (PMIP), Geophysical Research Letters, 26, 859–862, https://doi.org/10.1029/1999GL900126, 1999.

Kaufman, D., McKay, N., Routson, C., Erb, M., Davis, B., Heiri, O., Jaccard, S., Tierney, J., Dätwyler, C., et al.: A global database of Holocene paleo-temperature records, Scientific Data, in press.

Kaufman, D., McKay, N., Routson, C., Erb, M., Dätwyler, C., Sommer, P., Heiri, O., and Davis, B.: Holocene global mean surface temperature: a multi-method reconstruction approach, submitted.

New, M., Hulme, M., and Jones, P.: Representing twentieth-century space–time climate variability. Part II: Development of 1901–96 monthly grids of terrestrial surface climate, Journal of Climate, 13, 2217–2238, https://doi.org/10.1175/1520-0442(2000)013<2217:RTCSTC>2.0.CO;2, 2000.

Taylor, K. E.: Summarizing multiple aspects of model performance in a single diagram, Journal of Geophysical Research: Atmospheres, 106, 7183–7192, https://doi.org/ 10.1029/2000JD900719, 2001.

Xie, P. and Arkin, P. A.: Global precipitation: A 17-year monthly analysis based on gauge observations, satellite estimates, and numerical model outputs, Bulletin of the American Meteorological Society, 78, 2539–2558, https://doi.org/10.1175/2008JAMC1921.1, 1997.

Table S1. Key metrics of change in the PMIP4-CMIP6 *midHolocene* simulations

	Extratropical						Tropical						
	Global mean temperature (°C)	Summer NH high-lat. land (°C)	Drier Eastern North America (mm/yr)	Midcontinental Eurasia rainfall (mm/yr)	Midcontinental Eurasia Seasonality (°C)	Central Asian Seasonality (°C)	N. African monsoon expansion (°N)	Drier South America (mm/yr)	Indo-Gangetic rainfall (mm/yr)	Niño3.4 Variance‡ (%)	p(suppressed ENSO) in *piControl*§ (%)	p(suppressed ENSO) in *midHolocene*§ (%)	Eq. Pac SST gradient‡ (%)
AWI-ESM-1-1-LR	-0.5	0.2	-44	-25	2.6	2.9	3.2	140	82	-41	–	–	-10
CESM2	-0.1	1.1	-51	-16	2.8	3.1	2.7	-95	92	-16	2.4	5.7	-7
FGOALS-f3-L	-0.4	1.1	-6	-18	3.0	3.0	1.9	-91	170	4	–	–	0
FGOALS-g3	-0.2	2.3	-34	-67	4.2	4.1	1.1	-261	42	-14	–	–	-1
GISS-E2-1-G	-0.4	1.1	-14	-8	2.4	2.6	1.6	-61	170	2	1.8	5.6	4
HadGEM3-GC31	-0.1	1.2	16	-21	3.0	3.8	3.9	-103	193	-8	–	–	-3
INM-CM4-8	-0.3	1.1	24	-2	2.7	3.1	2.1	-96	211	7	1.5	14.2	-4
IPSL-CM6A-LR	-0.4	1.1	-12	-27	3.5	3.0	0.8	-71	158	-13	1.7	3.4	-3
MIROC-ES2L	-0.5	0.9	30	-26	2.8	3.4	0.9	-97	-108	-49	7.3	82.4	16
MRI-ESM2-0	-0.2	1.0	-24	-16	2.5	2.7	1.3	-178	176	-36	–	–	0
NESM3	-0.3	1.1	61	22	2.6	2.5	3.7	-182	-161	-24	2.1	5.2	-4
NorESM1-F	-0.4	0.9	6	-19	3.4	3.6	1.5	-118	149	-6	–	–	-6
UofT-CCSM-4	-0.2	1.6	-10	10	3.1	2.8	0.4	-326	27	-48	–	–	-2
Reconstructed	0.5†	0.7*	-93¶	121¶	–	–	–	–	–	–	–	–	–
PMIP4 Average	-0.3	1.1	-4	-16	3.0	3.0	1.9	-118	133	-19	–	–	-2
PMIP3 Average	-0.1	1.3	-11	-5	2.6	2.9	1.8	-83	166	-11	–	–	-3
PMIP3 Spread	0.2	0.4	16	15	0.4	0.4	2.1	44	75	14	–	–	6

†Median reconstructed global mean value from Kaufman et al. (submitted), with 80% confidence interval of 0.3–0.9 °C. *average of the difference in summer and winter reconstructions within the region from Kaufman et al. (in press) compilation. ¶average of reconstructions within the region from Bartlein et al. (2011) compilation. ‡Values published in Brown et al. (submitted). §using the analysis approach of Emile-Geay et al. (2016).

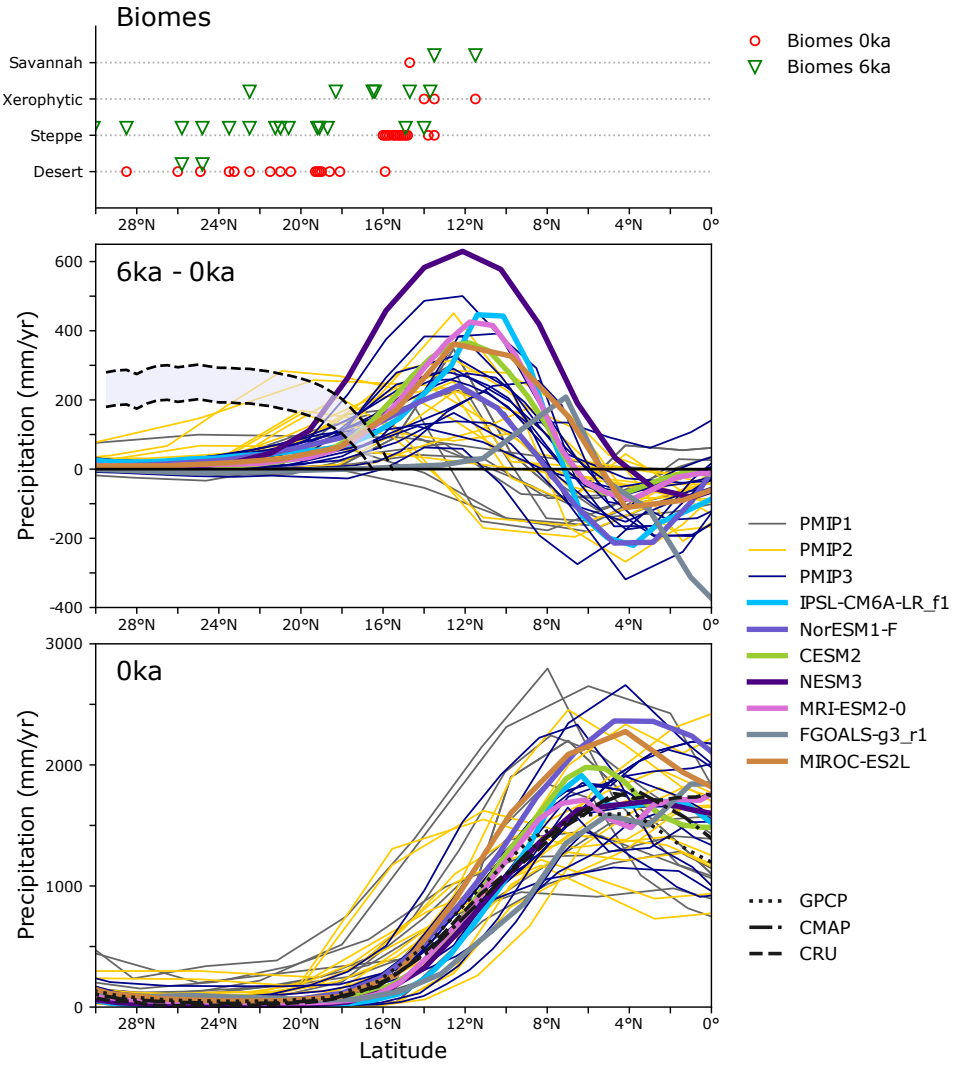

Figure S1. Simulated North African monsoon through multiple phases of PMIP-CMIP. (top panel) Biome distributions (desert, steppe, xerophytic and savannah/dry tropical forest) as a function of latitude for present (red circles) and 6 ka (green triangles), showing that steppe vegetation replaces desert at 6 ka as far north as 23°N (middle panel) Annual mean precipitation changes (mm/yr) over Africa (20°W–30°E) for the Mid-Holocene climate across multiple PMIP generations. The black hatched lines are estimated upper and lower bounds for the excess precipitation required to support grassland, based on present climatic limits of desert and grassland taxa in palaeo-ecological records. (bottom panel) The rainfall distribution in piControl simulations for each model. Three different observationally-based datasets are shown in black: GPCP (Adler et al., 2003), CMAP (Xie and Arkin, 1997), and CRU (New et al., 2000). (Adapted from Joussaume et al., 1999; Braconnot et al., 2007, 2012)

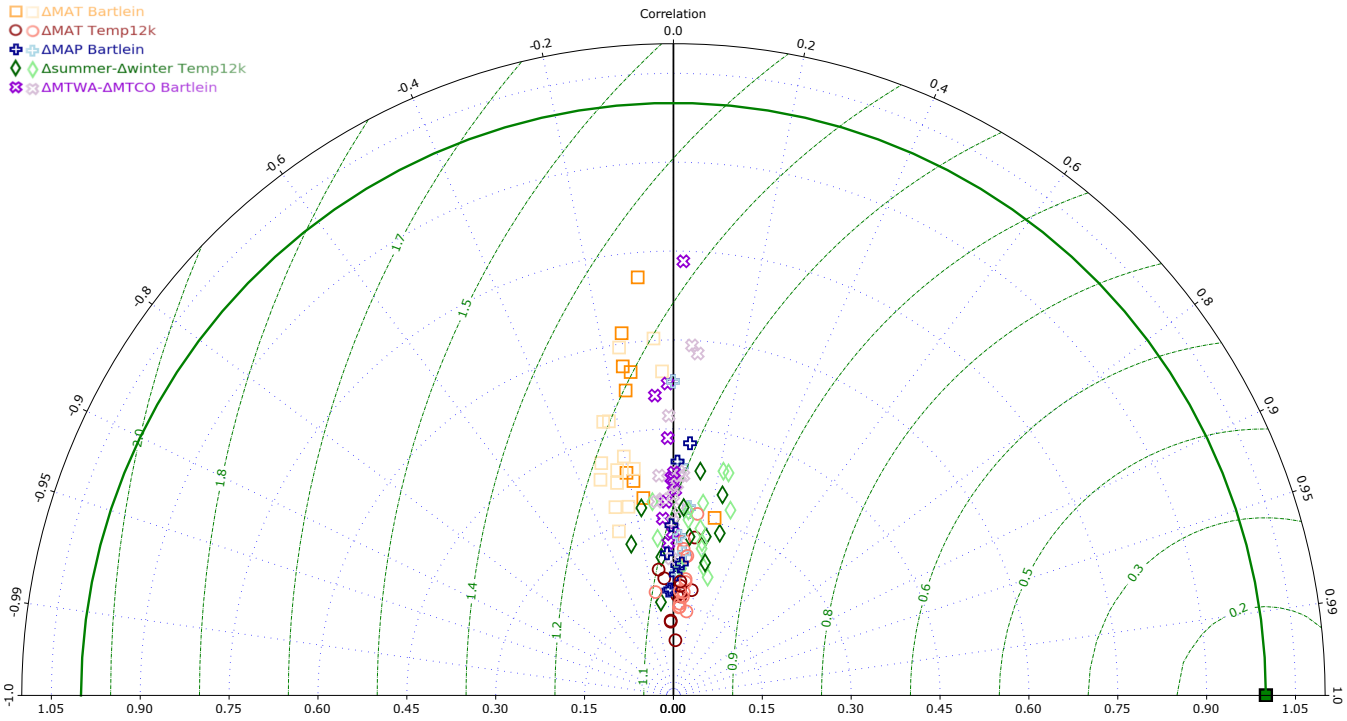

Figure S2. Statistical description of site-level comparison of simulated mid-Holocene climate changes to reconstructions. The performance of both the CMIP6 and CMIP5 ensembles are assessed by comparing the annual mean temperature changes and difference between summer mean temperature changes and winter mean temperature changes to multi-proxy Temperature 12k database (red, green; Kaufman et al., in press) and mean annual precipitation and difference between mean tempeature fo the warmest month (MTWA) changes and mean tempeature fo the coldest month (MTCO) changes to the pollen-based reconstructions (yellow, blue, purple; Bartlein et al., 2011). The better a model's changes fit with the reconstructions, then closer it should be to the green square. The correlation coefficient is plotted on the azimuth, and the standard error determines the radial distance (Taylor, 2001). The radial distance is adjusted to account for the existence of uncertainty in the reconstructions (after Hargreaves et al., 2013).

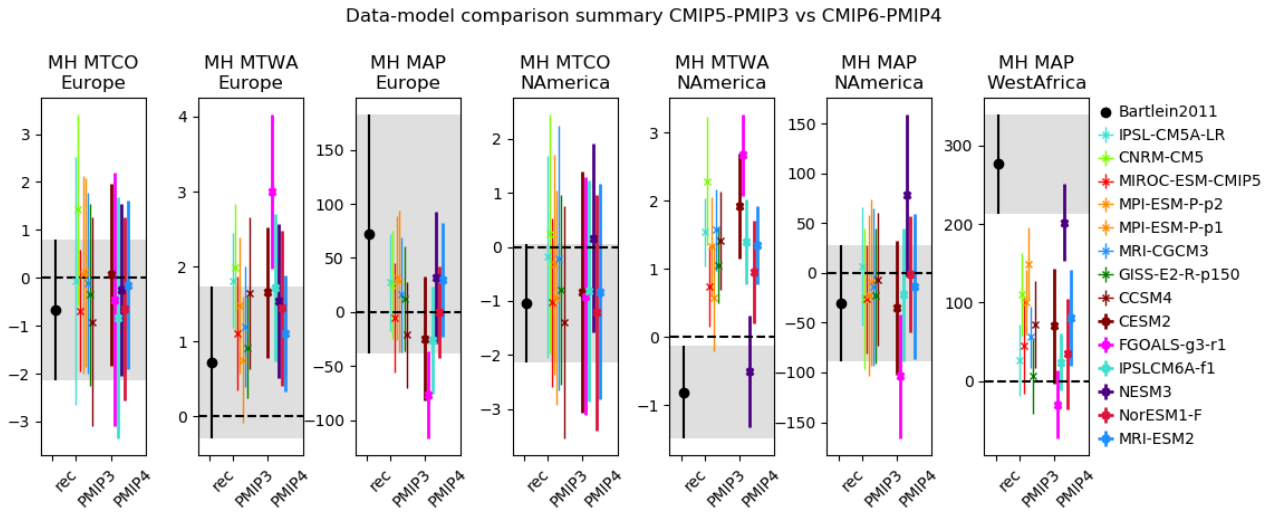

Figure S3. Alternate presentation of the data-model comparison. Regional comparisons using Monte-Carlo sampling of both the reconstruction uncertainty (Bartlein et al., 2011) and model uncertainty as expressed by interannual variability at individual proxy locations. The regions are defined as Europe (35–70°N, 10°W–30°E), West Africa (0–30°N,30°W–30°E) and North America (20–50°N,140–60°W)